Demonstrating the capabilities of an open-source simulation framework for positive displacement compressors and expanders

Davide Ziviani[a,*], Ian H. Bell[b], Xinye Zhang[a], Vincent Lemort[b], Michel De Paepe[c], James E. Braun[a], Eckhard A. Groll[a]

[a] *Ray W. Herrick Laboratories, School of Mechanical Engineering, Purdue University, 177 S. Russell Street, West Lafayette, IN 47907-2099, US*

[b] *University of Liège, Energy Systems Research Unit, Liège, Belgium*

[c] *Department of Flow, Heat, and Combustion Mechanics, Ghent University - UGent, Sint-Pietersnieuwstraat 41, 9000 Gent, Belgium*

Abstract

In this paper, the first open-source generalized simulation framework for positive displacement machines (PDSim) reported in literature is employed to model different compressor and expander types. In particular, it is shown how PDSim handles specific numerical and modeling aspects common to positive displacement machines such as stiffness of differential equations, discontinuous volume curves, leakage flow models, in-chamber and shell heat transfer models, mechanical and frictional losses. A control volume approach based on a set of differential equations is used to predict the performance of different positive displacement machines under steady-periodic operations. Reciprocating, scroll, and two rotary compressors as well as a single-screw expander have been considered as examples. The source code of PDSim with examples are provided as an electronic annex.

Keywords:
Positive displacement machines, Compressors, Expanders, Mechanistic models, Open-source, PDSim

1. Introduction

Improving the performance of positive displacement (PD) compressors and expanders for vapor compression systems or power generation systems has been one of the drivers for both academic research and industry development for many decades. Recent concerns regarding energy resource depletion and environmental issues such as global warming, require further improvements in system and component performance. Although vapor compression and power generation, *e.g.*, organic Rankine cycles, systems consist of several components, the compressor and expander are the most important ones because they consume or produce the greatest work associated with the system.

In order to investigate the feasibility and potential performance improvements of new PD machine designs, computer-based simulation models of different complexity have been developed and validated throughout the years. A particular class of PD machine models referred to as mechanistic models (also known as deterministic or chamber models) is particularly suitable to predict the actual performance at both design and off-design conditions and to quantify the losses (Soedel, 1972; Hamilton, 1974). Mechanistic models are based upon describing the working chamber(s) of a compressor or expander and their housings by means of open control-volumes to which a set of governing differential equations, *i.e.*, continuity, energy and momentum balance equations, is applied throughout a complete working cycle (Incropera and Dewitt, 2002). An open control-volume approach allows for the accounting of mass and energy transfer through the boundaries as well as internal heat and mechanical losses and the heat transfer with the surroundings.

It is well known that mechanistic models of PD machines present a common structure that can be tailored as needed to different type of machines (reciprocating, scroll, screw, rotary, among others) and can include different sub-models such as leakage flows, heat transfer and friction/mechanical losses. A general approach to PD compressor modeling was initially described in detail by Soedel (1972) and Hamilton (1974). Prankash and Singh (1974) applied such methodology to model a single cylinder reciprocating compressor for refrigeration including the cylinder working chamber, suction and discharge volumes as well as the associated pipe lines. The model included heat transfer in the cylinder, mass transfer through the valves, valve dynamics and the kinematics of the compressor. This approach was further extended to include gas pulsations (Zhou et al., 2001). Reciprocating compressors and rotary

*Corresponding Author
Email addresses: dziviani@purdue.edu (Davide Ziviani), ian.h.bell@gmail.com (Ian H. Bell), Zhan1600@purdue.edu (Xinye Zhang), vincent.lemort@ulg.ac.be (Vincent Lemort), michel.depaepe@ugent.be (Michel De Paepe), jbraun@purdue.edu (James E. Braun), groll@purdue.edu (Eckhard A. Groll)

NOMENCLATURE

A	Cross-sectional area (m^2)
b	Piston ring thickness (m)
c_v	Spec. heat at const. volume (kJ kg^{-1} K^{-1})
D	Diameter (m)
f	Friction factor (-)
F	Force (N)
$\mathbf{F}$	Force vector (N)
h	Specific enthalpy (kJ kg^{-1})
	Oil film thickness (m)
k	Thermal conduct. (kW m^{-1} K^{-1})
k_s	Valve spring coefficient (N m^{-1})
L	Length (m)
m	Mass (kg)
$\dot{m}_i$	Mass flow rate flow path (kg/s)
$\mathbf{n}$	Unit normal vector (-)
N_{motor}	Motor rotational speed (rpm)
p	Pressure (kPa)
$\dot{Q}$	Heat transfer rate (kW)
$\mathbf{r}$	Position vector (m)
R	Thermal resistance (K W^{-1})
Re	Reynolds number (-)
t	Time (s)
T	Temperature (K)
u	Specific internal energy (kJ kg^{-1})
U	Total internal energy (kJ)
	Velocity (m s^{-1})
	Natural vibration mode (-)
V	Volume (m^3)
$\dot{W}$	Power (kW)
$\dot{W}_{compr,sh}$	Compressor shaft power (kW)
y	Valve position (m)
μ_{oil}	Oil viscosity (Pa s)
μ_{fr}	Friction coefficient (-)
ω	Rotational speed (rad s^{-1})
θ	Crank angle (rad)
ρ	Density (kg m^{-3})
τ	Torque (N m)

compressors were mainly considered in their studies.

Since then, the complexity and comprehensiveness of the mechanistic models have increased making it possible to account for several physical phenomena occurring during the operation of the compressors and expanders. For example, Yang et al. (2013) included detailed models for the frictional losses at the bearings and between the piston rings and the cylinder wall in a semi-hermetic reciprocating compressor. Damle et al. (2011) developed an object-oriented unstructured modular simulation model of a reciprocating compressor by discretizing the compressor in different elements that formed the different control volumes. To each element, the conservation of mass, energy and momentum were applied. A global thermal analysis between the compressor elements was also included. More recently, chamber models have been coupled with FEM (finite element method) analyses or CFD (computational fluid-dynamics) simulations to improve the accuracy of the models. For instance, Stiaccini et al. (2016) included an acoustic FEM simulation into the compressor thermodynamic model to accurately predict the pressure pulsations in the compressor head due to valve motions. Similarly, Papes et al. (2016) introduced a coupling between a mechanistic model of a twin-screw expander and a 3D CFD inlet pipe model to capture the high gas pulsations at the inlet port and to improve the throttling losses.

The majority of the models proposed in the literature are developed for a particular type of positive displacement machine and not available open-source to other researchers (Stosic et al., 2011; Hu et al., 2014). A non-exhaustive list of mechanistic models of PD compressors and expanders reported in the literature is provided in Bell et al. (2019). An effort to compare different compressor types with the same modeling approach was done by Pandeya (1978). In particular, three compressors were studied: rotary vane, rolling-piston and reciprocating compressors. However, a cyclic averaging approach was adopted rather than a time step based model to reduce the computational resources needed. To the author's knowledge, this is the first time that a generalized simulation framework, namely PDSim (Positive Displacement Simulation tool), has been developed for all types of PD compressors and expanders. While the mathematical fundamentals of the simulation tool are described in Bell et al. (2019), this paper focuses on its capabilities of handling different numerical issues and modeling challenges that can be typically found in positive displacement machines. The present work provides a review of positive displacement compressor and expander mechanistic models. The source code of PDSim is made available to the scientific community.

2. Generalized structure of a mechanistic model for positive displacement machines

The mechanistic model of a generic PD machine can be divided into a certain number of blocks for which specific sub-models are required:

- definitions of control volumes (both static and dynamic) and their geometries in terms of $V(\theta)$ and $\mathrm{d}V/\mathrm{d}(\theta)$;
- leakage paths and their flow models;
- in-chamber heat transfer model;
- mechanical and friction losses;
- motor losses in semi-hermetic and hermetic machines;
- shell thermal network and overall energy balance;

- thermophysical properties and multi-layer solution scheme.

Compression and expansion processes in PD machines are transient thermodynamic processes. Therefore, to be studied, a system of transient conservation equations is necessary. Each working chamber is described thermodynamically by means of open control volumes (Incropera and Dewitt (2002)). Each control volume (CV) is assumed to have uniform thermodynamic properties, which implies also quasi-equilibrium conditions. This approach has been proven to be accurate enough to predict the performance of PD machines (Soedel (1972)). Non-uniformity of the thermodynamic properties within the chamber volume can be accounted for by means of CFD methods. The following hypotheses are applied to a general CV:

- uniform temperature and pressure throughout the control volume;
- negligible kinetic energy of the control volume;
- negligible gravitational effects;
- thermal interaction possible through heat transfer;
- mass flow into or out of control volume.

More detailed information about the mathematical formulation of the governing equations and sub-models can be found in Bell et al. (2019).

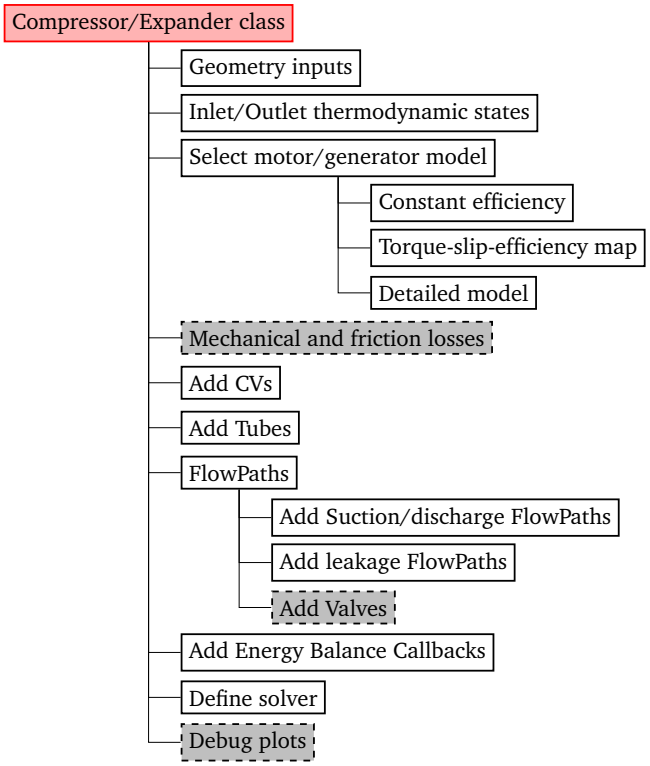

Figure 1: General class of a compressor/expander model in PDSim. Dashed boxes represent optional elements of a compressor/expander simulation model.

3. PDSim Framework

In the following sub-sections, the details of the implementation of PDSim are described.

3.1. Implementation

PDSim has been developed in the Python programming language with support for both 2.x and 3.x distributions. The adoption of Python is justified by its open-source and cross-platform nature, the numerous packages available and the active community. PDSim takes advantage of both the high-level features of Python as well as the low-level code through Cython (Behnel et al., 2011) to achieve higher computational efficiency. PDSim is coded in an object-oriented fashion that ensures a plug-and-play structure that simplifies the construction of a model and facilitates the extension of the existing libraries. Additionally, PDSim integrates GUI (Graphical User Interface) development through the wxPython package. Each family of positive displacement machines represents a class in PDSim that can be used to build a specific compressor or expander model. The general structure of a class of a simulation model in PDSim is shown in Figure 1 and it follows the typical work process of building a mechanistic model of a PD machine. The source code of PDSim consists of three main folders:

- *PDSim*: holds all the core elements to build a model and the different classes of PD machines. The PDSim folder includes the following sub-folders:
  - *core*: includes the core elements of PDSim (e.g. governing equations, overall solution scheme, general methods);
  - *flow*: includes all the flow models and flow path methods;
  - *misc*: includes miscellaneous items that can be useful while developing models;
  - *plot*: includes the plotting classes for the debug plot features of PDSim;
  - *recip*: includes the reciprocating machine core class;
  - *rolling*: includes the rolling-piston machine core class;
  - *scroll*: includes the scroll machine core class;
- *GUI*: includes the files for the graphical user interface.
- *examples*: includes the examples of compressors and expander codes.

For a given machine type, the corresponding core class is derived from the main *PDSimCore* class (located at PDSim/core/core.py) and inherits a number of methods that allow the actual model to be run with minimal coding required. These methods are:

- *add_CV( )*: add the control volumes;
- *add_flow( )*: add the flow paths (inlet and outlet flows, suction and discharge flows, leakage flows);

Table 1: Main parameters of the compressors and expander presented in this paper

Type	Parameter	Value	Notes
Reciprocating	Number cylinders	2	
	Piston diameter	44 mm	
	Stroke	12.5 mm	
	Crank length	6.25 mm	
	Connecting rod length	51 mm	
	Working fluid	R-410A	
	Lubricant oil	POE 32	
Scroll	Volume ratio	3.3	
	Max displaced volume	83 cm^3	2 Arcs discharge profile
	Working fluid	R-410A	
Rolling-piston	Cylinder radius	27 mm	
	Roller Radius	23.4 mm	
	Eccentric inner radius	18 mm	
	Eccentricity	4.8 mm	
	Cylinder height	28 mm	
	Vane thickness	4.7 mm	
	Working fluid	R-410A	
Z-	Working fluid	Air	Ziviani and Groll (2017)
Single-screw	Working fluid	R-245fa	Ziviani et al. (2016)

- *add_tube( )*: add inlet and outlet tubes of the compressor/expander as well as possible injection lines;
- *add_valves( )*: add valves, if any.

The pseudo-code of a simple compressor model in a Python-like style is shown in Figure 2.

3.2. Steady-periodic modeling

There are a variety of PD compressors and expanders where the working principle is based upon the crank angle. Generally, three families can be identified:

- reciprocating type, *e.g.*, piston, swash-plate or wobble-plate, S-RAM
- rotary type, *e.g.*, rolling-piston, sliding vane, spool, screw;
- orbital type, *e.g.*, scroll, trochoidal, Wankel.

Three compressor types have been identified to be representative of conventional compressor technologies for residential, commercial, and industrial applications. A fourth compressor has also been considered as a novel compression technology. Each compressor presents unique modeling features that will be addressed by utilizing PDSim:

- Reciprocating compressor: multiple cylinders and valves, piston-ring lubrication model, detailed motor model, multi-lumped temperature energy balance.
- Scroll compressor: merging and splitting of multiple control volumes and detailed model of forces and moments.
- Rolling-piston compressor: multiple friction losses and and leakage flows.

Figure 2: Compressor pseudo-code in a Python-like style

```
# Instantiate the model
comp = CompressorClass()
# Define the inputs}
# For example: comp.Vdead = 0.5e-5}
# Define boundary conditions}
Ref='Air'
inletState = State(Ref, T=298.15, P=101.325)
outletState = State(Ref, P=2*inletState.P, S=inletState.S)
mdot_guess = inletState.rho*comp.Vdisp*comp.omega/(2*pi)
# Add control volume(s)
comp.add_CV(ControlVolume(key, inletState, VdVFcn, becomes))
# Add inlet tube
comp.add_tube(Tube(
    key1='inlet.1', key2='inlet.2', L, D,
    mdot=mdot_guess, State1=inletState.copy(),
    fixed=1, TubeFcn=comp.TubeCode
))
# Add outlet tube
comp.add_tube(Tube(
    key1='outlet.1', key2='outlet.2', L, D,
    mdot=mdot_guess, State2=outletState.copy(),
    fixed=2, TubeFcn=comp.TubeCode
))
# Add flow paths to link flow nodes}
comp.add_flow(FlowPath(key1,key2,MdotFcn))
comp.add_flow(FlowPath(key1,key2,MdotFcn))
# Connect all the callbacks
comp.connect_callbacks(
    endcyle_callback=comp.endcycle_callback,
    heat_transfer_callback=comp.heat_transfer_callback,
    lump_energy_callback=comp.lump_energy_callback
)
# Run the solver
comp.solve(
    key_inlet='inlet.1',
    key_inlet='outlet.2',
    solver_method='RK45',
    OneCycle = False,
    UseNR = False
    )
```

- Z-compressor: multiple control volumes with phase shift, several friction and leakage losses, detailed multi-lumped temperature energy balance.

3.3. Extension to dynamic modeling

The steady-periodic formulation outlined in Section 3.2 presents limitations with respect to the ability of predicting the dynamic characteristics of a PD machine. Dynamic behaviors occur during operation for a number of different reasons. However, in order to generalize the problem statement, three categories can be identified as follows:

- transient operation of a PD machine, *e.g.*, start-up and shut-down or multi-staging compressors;
- intrinsically dynamic characteristics of a PD machine due to vibrations, gas pulsations, non-fully cyclic conditions;
- dynamic characteristics of the working principle of a specific machine, *e.g.*, linear compressors.

With respect to modeling transients, Link and Deschamps (2011) proposed a comprehensive model of a reciprocating compressor to predict the start-up and shut-down operations. The model accounted for the cycle to cycle variations in the gas dynamics through suction and discharge systems, in the compression chambers as well as in the dynamics of the bearings. The transients of the compressor lumped mass temperatures were neglected due to their larger time scale compared to the in-cylinder thermodynamic process. The compressor model was solved by discretizing the system of differential equations through a finite volume methodology. The pressure time variation in the suction and discharge lines was obtained from experimental data. In order to predict the pressure fluctuations in the suction and discharge lines, gas pulsation models based on acoustics theory should be included. For instance, Zhou et al. (2001) presented a detailed reciprocating compressor model with an improved iteration scheme that allowed the gas pulsation model and the in-cylinder thermodynamic model to be solved in the frequency domain and in the time domain (so called two-domain method), respectively. The four-pole method implemented to predict the gas pulsations was the result of the extensive work carried out by Soedel and Hamilton on noise and vibration in positive displacement compressors (Soedel, 2007; Zhou et al., 2001). Although both the transients and gas pulsations are important aspects of dynamic compressor modeling, they are beyond the scope of the present work. In the case of linear compressors, the stroke is determined by dynamically balancing electromagnetic, spring and gas forces to ensure operation close to the system resonance frequency, as described by Kim et al. (2009).

In PDSim, the core governing equations have been implemented both in the crank angle-domain and in the time-domain in order to be able to also analyze the steady-periodic and dynamic behavior of a compressor, respectively.

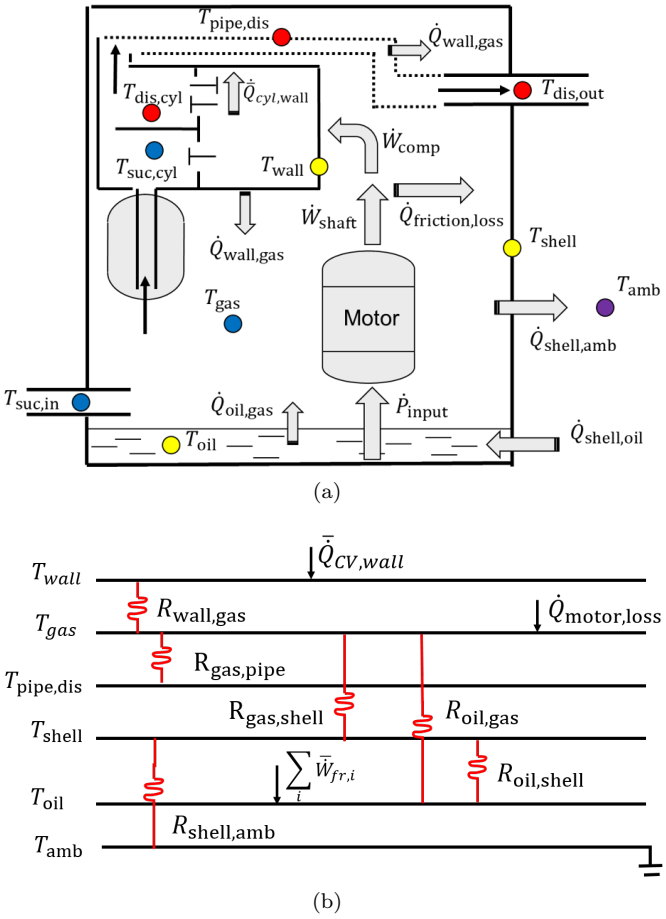

Figure 3: Hermetic single-cylinders reciprocating compressor (*a*) compressor shell schematic; (*b*) overall energy balance thermal resistance network.

The present work limits its scope to crank-based compressor types. Nevertheless, details of a linear compressor dynamic model that makes use of the versatile PDSim structure have been described by Zhang et al. (2017) including the coupling between mechanical and electric parts (Kim et al., 2009) as well as a dynamic thermal model for the compressor shell energy balance (Liu, 1994).

4. Examples of Compressor and Expander Models

The simulation tool PDSim is utilized to simulate four different compressor types and an expander to showcase its versatility. The models considered in the following subsections have been previously coded in other programming languages and published in the literature. The main geometric parameters of all the compressors considered in this work are grouped conveniently in Table 1.

4.1. Reciprocating compressor

Simulation models of reciprocating compressors and their components are well covered in the literature. PDSim

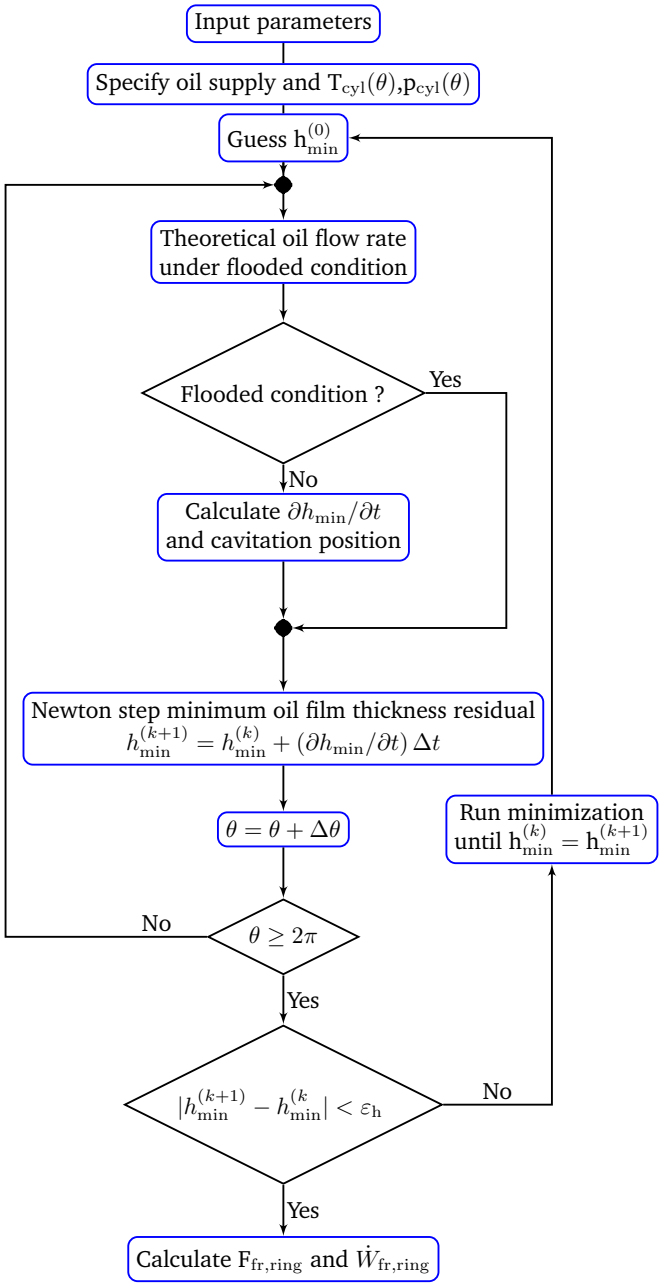

Figure 4: Algorithm of piston ring model. Adapted from (Nakai et al., 1996)

is employed to build a comprehensive model of a hermetic R-410A reciprocating compressor based on a previous model developed and validated by Yang et al. (2017). The schematic of the compressor is shown in Figure 3(a). This model includes sub-models for the kinematics, compression process, frictional power loss, and an overall energy balance with detailed thermal network, shown in Figure 3(b). In addition, the in-cylinder heat transfer model, leakage model and valve model are included in the compression process model. Both the frictional power losses at the piston ring and bearings are considered. Although such sub-models are described in detail in the literature, some key modeling aspects are highlighted.

Both the suction valves and discharge valves are reed-type. Usually valves can be modeled with a single-degree-of-freedom lumped approach or by applying statics analyses. However, the motion of the reed valve subjected to the gas pressure difference across the valve can be approximated as a motion of a cantilever beam exerted by the same force. The fundamentals of this approach has been extensively described by (Soedel, 2007) and it is based on the transverse displacement of a cantilever beam. The solution, $u(x,t)$, of the instantaneous transverse displacement of the valve at a certain position x along the valve is expressed as the combination of infinite modal series:

$$u(x,t) = \sum_{k=1}^{\infty} \eta_k(t) U_k(x) \tag{1}$$

where $U_k(x)$ is the *k-th* natural vibration mode and $\eta_k(t)$ is the time varying weight factor corresponding to the *k-th* natural vibration mode. Examples of such analysis have been presented by Ooi et al. (1992) and Yang et al. (2017).

One of the major contributions to the friction losses in a reciprocating compressor is caused by the piston ring which is located between the piston and the cylinder wall to seal the in-cylinder working fluid. Mixed lubrication theory with the effect of surface roughness has been applied to study the piston ring-cylinder wall lubrication problem. In particular, the model proposed by Yang and Zhao (2013) has been extended by including flooded and non-flooded conditions as described by Nakai et al. (1996). The solution algorithm of the lubrication problem of the piston ring-cylinder is shown in Figure 4. Once the oil film thickness, h, is obtained by integrating the Reynolds equation, the friction force between the piston ring and the cylinder liner can be calculated as a function of the oil viscous shear force and the asperity contacts:

$$F_{fr,piston-ring}(\theta) = sign(U(\theta)) \left[\int_{-b/2}^{b/2} \frac{\mu_{oil}|U(\theta)|}{h(\theta)} dx + \mu_{fr} W_A \right] \tag{2}$$

where U is the instantaneous piston velocity, b is the piston ring thickness, W_A is the asperity contact force, μ_{oil} is the oil dynamic viscosity, h is the instantaneous oil film thickness, and μ_{fr} is the friction coefficient. The instantaneous frictional power loss is given by:

$$\dot{W}_{fr,piston-ring} = F_{fr,piston-ring}(\theta) U(\theta) \tag{3}$$

The average friction power loss over one complete working cycle is obtained as:

$$\overline{\dot{W}}_{fr,piston-ring} = \frac{N_{motor}}{60} \int_0^{2\pi} \dot{W}_{fr,piston-ring}(\theta) \frac{d\theta}{\omega} \tag{4}$$

where ω is the angular speed corresponding to the motor rotational speed N_{motor}.

In order to estimate the losses of the induction motor, an equivalent electrical circuit method as described by Dutra

and Deschamps (2015) has been implemented. The model accounts for the Joule-effect losses in the stator, the losses in the rotor windings, and the stator core losses. The model is solved iteratively to calculate the motor slip ratio to match the compressor shaft power. An example of single-phase induction motor torque and efficiency curves as a function of the rotational speed obtained with the motor model is shown in Figure 5. A few experimental data points have been also overlaid to show the correctness of the model.

An example of simulation results are shown in Figure 6 for evaporating and condensing temperatures of 5 °C and 35 °C. In the figure, the instantaneous in-cylinder pressure trace is reported along with the discharge and suction valve lifts. Figure 7 shows the oil-film thickness as a function of the crack-angle.

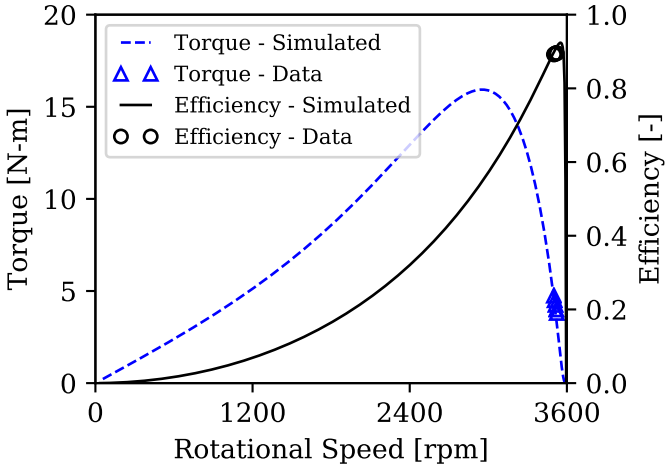

Figure 5: Example of outputs from the detailed induction motor model. Experimental data points obtained from the compressor manufacturer are overlaid to ensure the correctness of the model.

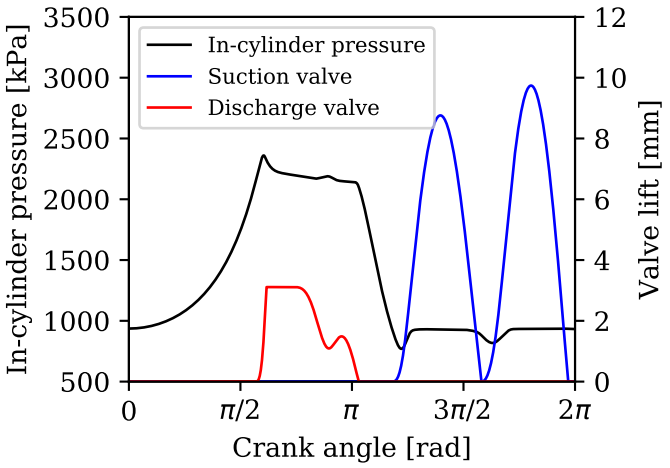

Figure 6: In-cylinder pressure and valve lifts of a reciprocating compressor.

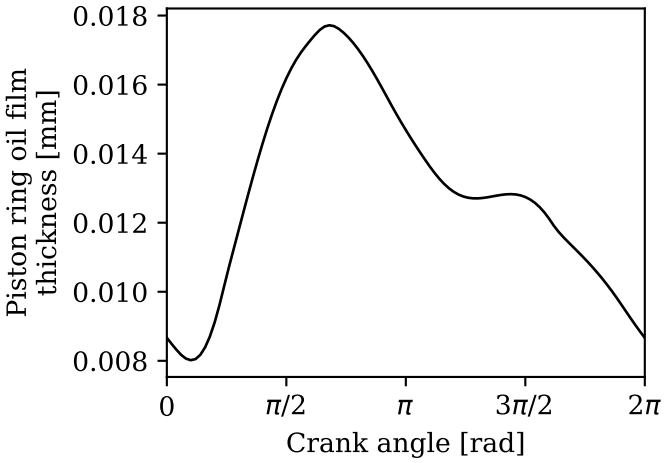

Figure 7: Piston-ring oil film thickness.

4.2. Scroll compressor

Scroll compressors are characterized by a fixed wrap and an orbiting wrap having an involute whose geometry is based on the form of an involute unwrapping from a circle. Due to the orbiting movement, the definitions of the compressor control volumes change continuously throughout the compression process, as shown in Figure 8. The mathematical formulation of the scroll geometry is quite involved and requires the calculation of the following quantities:

- volumes of all chambers as a function of the crank angle (Bell, 2011; Chen et al., 2002a,b; Halm, 1997; Lemort, 2008; Lemort et al., 2008);
- derivatives of the volumes of all chambers with respect to the crank angle;
- centroid of each chamber to evaluate the overturning moments due to gas forces;
- force components on the orbiting scroll due to pressure forces;
- radial leakage areas between chambers.

The complex shapes of the chambers are handled by introducing two types of area elements (triangles and parametrized curves) and the use of the Green's Theorem to obtain areas and volumes. The comprehensive geometric solutions derived by Bell et al. (2014a) have been implemented within PDSim. The variations of the control volumes over one rotation are shown in Figure 9 for completeness. The geometry model is integrated into the generalized simulation framework to calculate the performance of the compressor. The axial and radial leakage flows have been modeled by employing the hybrid method described in Bell et al. (2013a). In addition, injection ports can be added to investigate the effect of vapor or liquid injection on the compression process. Due to the complexity of a vapor-injected compressor models, the reader is invited to refer to Bell et al. (2013b) to have more in-depth description. Nevertheless, an example of a vapor-injected scroll compressor is provided as part of the source code.

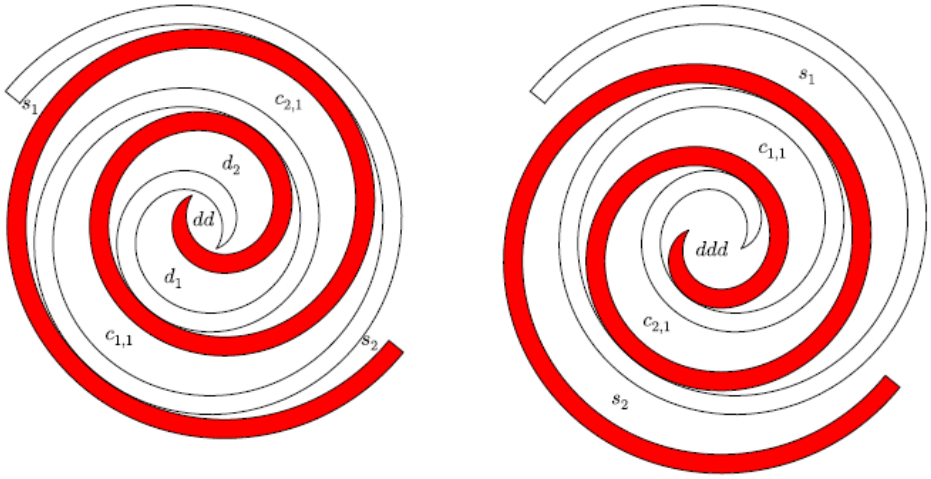

Figure 8: Definition of the scroll compressor working chambers.

Figure 10 shows an example of p-V diagram reconstruction for the scroll compressor. Once the thermodynamic model has converged, the pressure distribution in the chambers can be used to calculate the axial and radial loads and the moments. In particular, the differential of force vectors on the scroll wraps is given by

$$\frac{\mathrm{d}\mathbf{F}}{p} = \mathrm{dA} \cdot \mathbf{n} \tag{5}$$

where p is the instantaneous pressure in a working chamber, dA is the differential area over which the force is applied and $\mathbf{n}$ is the unit normal vector that points towards the scroll wrap. By integrating Equation 5, the right-hand side has a known solution from the geometry model (Bell et al. (2014a)). Therefore, the net force vector applied to the shaft can be expressed as the sum of the force contributions from each control volume:

$$\mathbf{F} = \sum_{\mathrm{CV=s1,s2,...}} \left(\frac{\mathbf{F}}{p}\right)_{\mathrm{CV}} p_{\mathrm{CV}} \tag{6}$$

Thus, the instantaneous torque induced by the gas loads can be obtained from

$$\tau = \mathbf{r} \times \mathbf{F} = \left(\mathbf{r}_x \mathbf{F}_x - \mathbf{r}_y \mathbf{F}_y\right) \hat{k} \tag{7}$$

where $\mathbf{r}$ represents the vector from the center of the shaft to the pin location at the end of the shaft. An example of the instantaneous torque is shown in Figure 11. By calculating the mean torque value over one rotation, it is possible to estimate the average power necessary to compress the gas as

$$\dot{W}_{\mathrm{compr,sh}} = \bar{\tau}\omega \tag{8}$$

The actual compressor input power is obtained by adding friction losses and motor losses, and accounting for the heat losses.

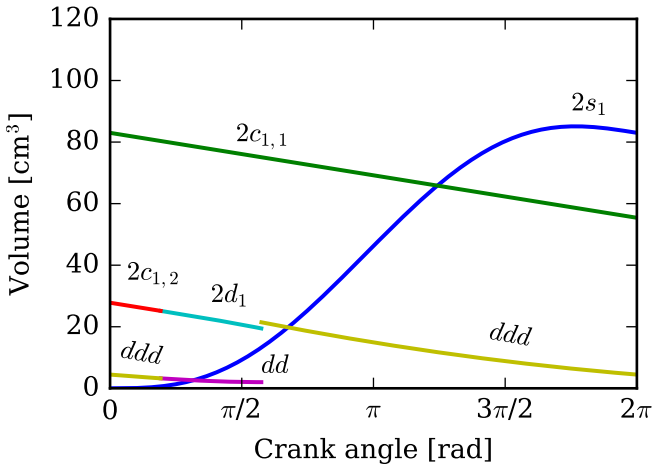

Figure 9: Variation of chamber volumes with the crank angle in a scroll compressor.

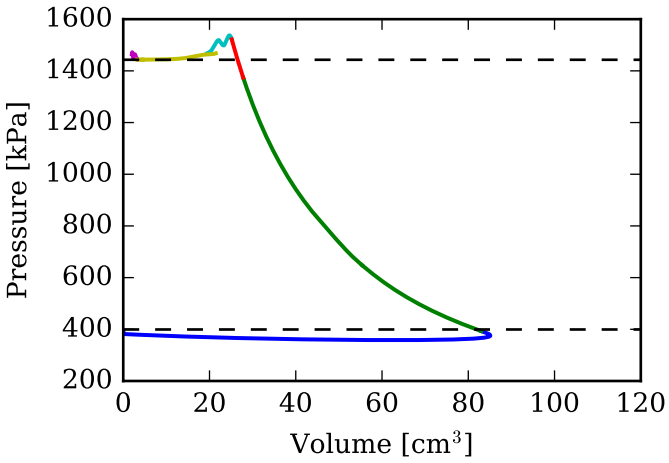

Figure 10: Scroll compressor p-V diagram.

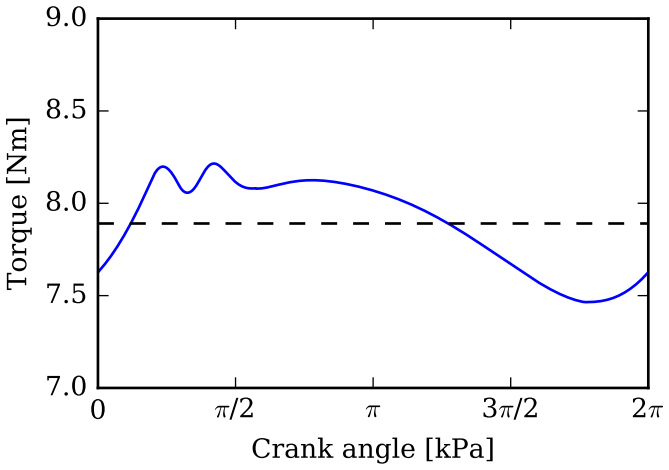

Figure 11: Mechanical torque of a scroll compressor.

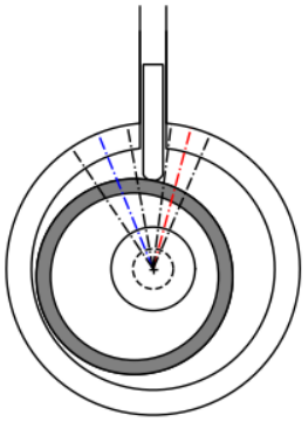

Figure 12: Rolling piston compressor geometry.

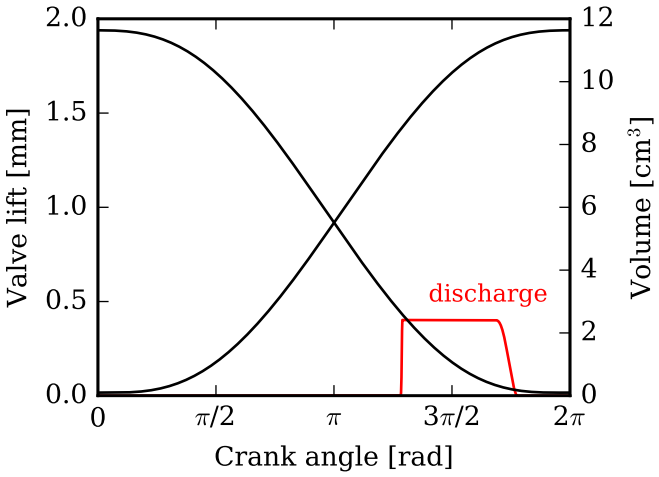

Figure 13: Compressor chamber volumes and discharge valve motion for a rolling piston compressor.

4.3. Rolling-piston compressor

The rolling-piston compressor consists of an eccentric roller located inside a cylinder and a vane that extends from the cylinder wall to the roller surface that separates suction and compression chambers, as shown in Figure 12. The rolling-piston compressor does not have a suction valve and the gas fills the suction chamber as its volume increases over an entire revolution of the roller. At the same time, the compression chamber decreases its volume, compressing the gas until the pressure is high enough to open the discharge valve. The model implemented in PDSim is based on the work done by Mathison et al. (2008) with the addition of friction analysis.

The mathematical description of the evolution of the chamber volumes as function of the crank angle is well known in the literature (Liu, 1994; Ooi and Wong, 1997; Mathison et al., 2008; Lee et al., 2015). An example of suction and discharge volume curves are illustrated in Figure 13. Other geometric quantities such as heat transfer surfaces, hydraulic diameters can be easily calculated as described by Mathison et al. (2008).

The complexity of building a mechanistic model of a rolling-piston compressor is associated with the multiple leakage paths and the multiple sources of friction losses. Extensive research on leakage flows in rolling-piston compressors can be found in the literature (Yanagisawa and Shimizu (1985b,c); Gasche et al. (2012); Wu and Chen (2015)). In the model presented here, the leakage flows are classified as proposed by Mathison et al. (2008). In particular, the isentropic flow model of compressible ideal gas is utilized to describe leakage flows from compression to suction chamber through radial clearance and from clearance volume to suction chamber where the mass flow rate is dependent on the pressure ratio across the flow path; a mixed Couette and Poiseuille flow model is used to model the flow along the sides of the sliding vane due to the effect of the vane motion that must be considered; a laminar viscous flow model is employed to model the leakage that occurs across the top of the rolling-piston where there are high concentrations of lubricant oil.

The typical mechanical structure of a rolling-piston compressor (both single- and two-cylinders) includes the main crankshaft with the roller, sub- and main bearings, lower and upper balancers, and the motor, as described by Zhang et al. (2014). In order to determine the different friction losses, the vane and the roller dynamics must be solved first. The equation of motion of the rolling-piston around its center and the analysis of the forces acting on the vane have been described by Yanagisawa et al. (1982). In the present model, it is assumed that the angular velocity of the rolling-piston is constant to simplify the analysis. Once the instantaneous forces and moments are computed, the following friction losses can be computed according to the formulation proposed by Yanagisawa and Shimizu (1985a) and Ooi (1992):

- between eccentric and the inner surface of the roller;
- between the roller face and the cylinder head face;
- between the eccentric face and the cylinder head face;
- between the vane tip and roller;

- between vane sides and vane slot;
- between the outer roller surface and the inner cylinder surface;
- at the bearings.

The rolling-piston model is closed with a single-lump shell energy balance. The compressor shell is approximated as a vertical cylindrical surface with two flat surfaces at the top and bottom. The heat losses through the shell are modeled by defining appropriate heat transfer coefficient for natural convection over a vertical cylinder and over horizontal surfaces according to Mathison et al. (2008) and Incropera and Dewitt (2002).

A typical p-V diagram is shown in Figure 14. In Figure 15, the instantaneous gas force, normal and tangential forces are overlaid. By computing the average values of the forces and moments, the distribution of frictional losses can be calculated, as illustrated in Figure 16.

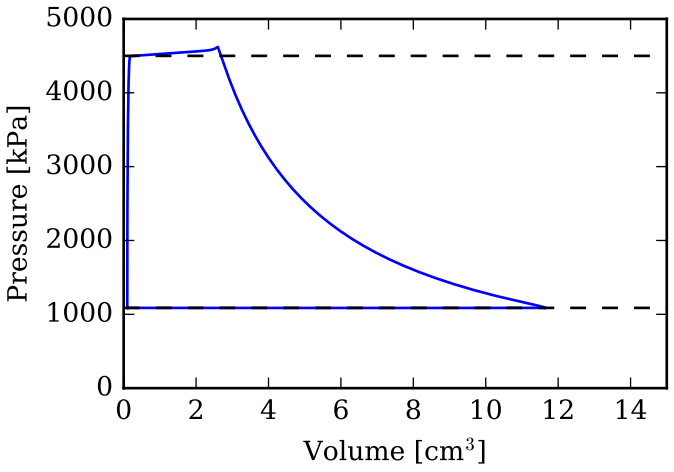

Figure 14: Rolling piston compressor p-V diagram.

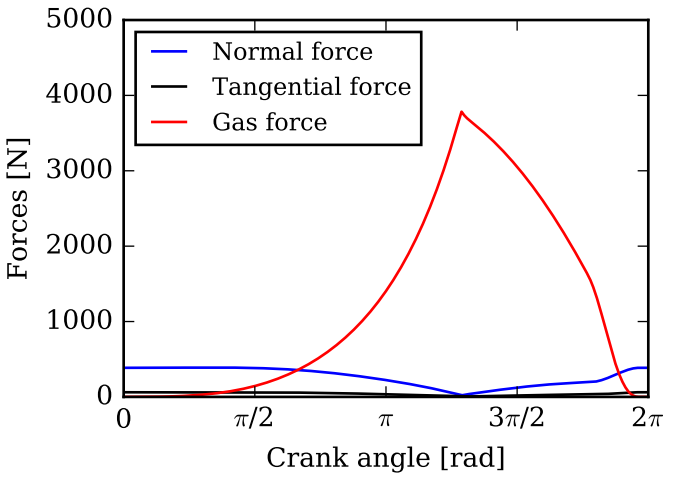

Figure 15: Decomposition of the forces in a rolling piston compressor.

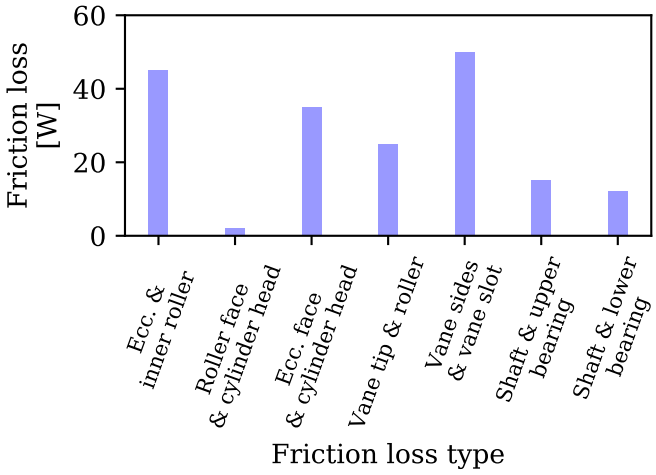

Figure 16: Friction losses in a rolling piston compressor.

4.4. Z-compressor

The Z-compressor represents a novel compressor that is within the family of rotary compressors. A cut-away view of the compressor is shown in Figure 17. The design concept resembles a two-stage rolling compressor and presents two sets of compression and suction chambers with a half revolution shift between the upper and lower level. The volume of the chambers is the space between inner and outer cylinder walls and the height of the chambers changes periodically as a function of the crank angle. The element that separates the upper and lower chambers is called the blade. Additionally, the chambers on the same side of the blade are separated by means of a point of zero height with the housing and by a sliding vane. Due to the shape of blade and inner cylinder from a front view (see right side of Figure 17), the compressor is denoted as Z-compressor.

The Z-compressor was first analyzed by Jovane (2007) for refrigeration applications. Experimental work done on a hermetic prototype showed that the Z-compressor had low vibration and noise effects, but its performance was heavily affected by leakages and friction losses. A model of the dynamics of the Z-compressor was developed in order identify the important sources of losses, such as leakage, friction, and heat transfer and to optimize the geometry. The model was validated with internal and external experimental data generated using R-410A as the working fluid. More recently, Ziviani and Groll (2017) evaluated the feasibility of designing a miniature open-drive Z-compressor for air-compression applications. A comprehensive model was developed to assess the impact of leakage flows and frictional losses.

The miniature Z-compressor is considered to highlight how different modeling aspects are handled within PDSim. In particular the following challenging aspects can be identified for this particular compressor type:

- down-sizing of compressors implies greater influence of leakages and friction losses;

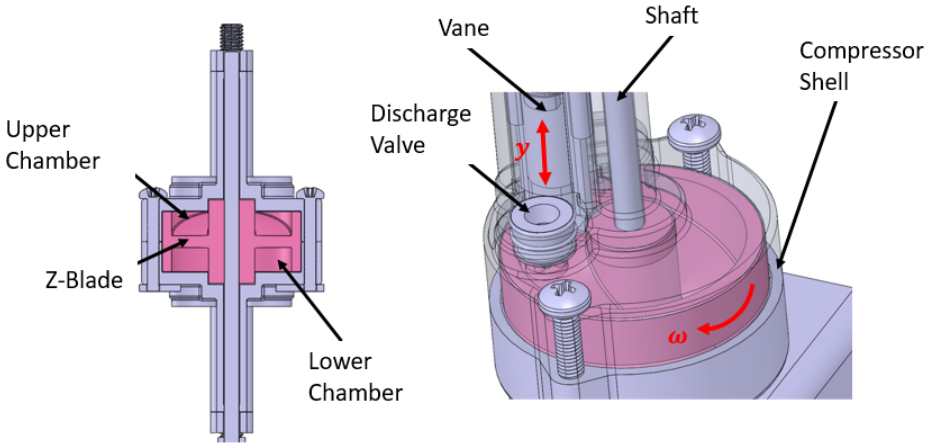

Figure 17: Z-compressor cutaway view with indicated upper and lower suction and compression chambers.

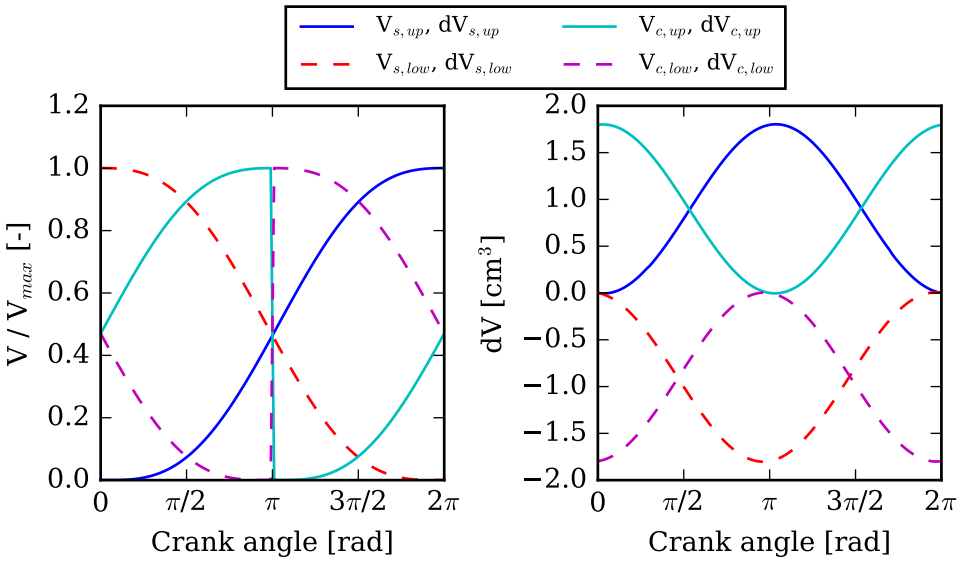

Figure 18: Z-compressor chamber volume curves and their derivatives as a function of the crank angle.

- multiple-control volumes and discontinuities in the volume curves;
- two discharge reed valves;
- multiple leakage paths with both constant and variable gap sizes;
- multiple sources of friction losses;
- steady-state overall energy balance with multiple lumped elements.

The open-drive Z-compressor design features two ports on each side of the compressor allowing for suction and discharge processes. Reed valves are installed on the discharge ports. The main design difference with respect to the original Z-compressor analyzed by Jovane (2007) is the blade integrated with the outer cylinder which avoids direct leakage paths from upper to lower chambers and vice-versa as shown in Figure 17.

The working process is similar to a twin rolling piston rotary compressor in which two compression processes occur in one rotation. Four working chambers can be identified: upper suction and compression chambers and lower suction and compression chambers as seen in the cutaway view shown in Figure 17. Differently from a rolling piston rotary compressor, the Z-blade allows for volume variations. Two sliding vanes separate suction and compression chambers located on the same side of the Z-blade. The volume of each chamber is the space between inner and outer cylinders and the height of the chambers is dictated by the height of the portion of the Z-blade in contact with the vane, y_b. The length of each portion of the vanes into the working chambers is given as:

$$y_{\text{up}}, y_{\text{low}} = \frac{h_b}{2}\left[1 \mp cos(\theta)\right] \tag{9}$$

where h_b is the maximum height of the Z-blade, the minus sign is used for the upper chambers (up) and the plus sign for the lower chambers (low) and θ is the rotation angle measured from the point of contact between the Z-blade

and the vane to the point at with the Z-blade has zero height with respect to the housing.

The volume of the suction and compression chambers in both sides of the Z-blade are obtained by defining a maximum chamber volume as

$$V_{\max} = \frac{\pi}{2} h_b \left(r_o^2 - r_i^2\right) \tag{10}$$

where r_o and r_i are the inner and outer radius of the Z-blade, and the vane volume within the chamber which is a function of the height of the chambers and the shape of the vane, i.e., $V_v = f(y(\theta),\text{geo})$. Therefore, the upper suction and compression chambers are given by,

$$V_{\text{s,up}} = \frac{V_{\max}}{2\pi} \left(\theta - \sin\theta\right) - V_{\text{v,up}}(\theta) \tag{11}$$

$$V_{\text{c,up}} = \frac{V_{\max}}{2\pi} \left(2\pi - \theta + \sin\theta\right) - V_{\text{v,up}}(\theta) \tag{12}$$

The lower suction and compression chambers are obtained from Equation 11 and Equation 12 by including the half revolution shift:

$$V_{\text{s,low}} = \frac{V_{\max}}{2\pi} \left(\pm\pi + \theta - \sin(\theta \pm \pi)\right) - V_{\text{v,up}}(\theta \pm \pi) \tag{13}$$

$$V_{\text{c,low}} = \frac{V_{\max}}{2\pi} \left(2\pi \mp \pi - \theta + \sin(\theta \pm \pi)\right) - V_{\text{v,up}}(\theta \pm \pi) \tag{14}$$

where the upper sign on Equation 13 and Equation 14 is used for $\theta \leq \pi$ and the lower sign for $\theta > \pi$.

The main dimensions of the Z-compressor are reported in Table 1. The evolution of the working chamber volumes and their derivatives are shown in Figure 18 and they can be integrated into the compression process governing equations. The Z-compressor is divided into five control volumes of which four are associated with upper and lower suction and compression chambers and their volumes change according to the rotation angle (see Figure 18). A fifth static control volume is introduced to account for the space between the rotating cylinder and the external housing as well as the space where the vanes are installed.

The mass flow rates through the discharge valves are estimated by applying a one-degree-of-freedom dynamic model to the reed valves having two operating modes, i.e., pressure dominant when the net force on the valve is dominated by the pressure difference across the valve, and mass flux dominant when the gas velocity is the dominant force (Bell et al., 2019).

As shown in Figure 18, the lower chambers are phased by a half rotation. As a consequence, there are two discontinuities in the volume curves when the rotation is at π. During the integration of the differential governing equations, such discontinuities would not allow the convergence of the code. This numerical issue has been handled by coupling an adaptive step-size solver with a *step-callback function* that helps the solver to step through the discontinuity by taking a sufficiently small step before and after

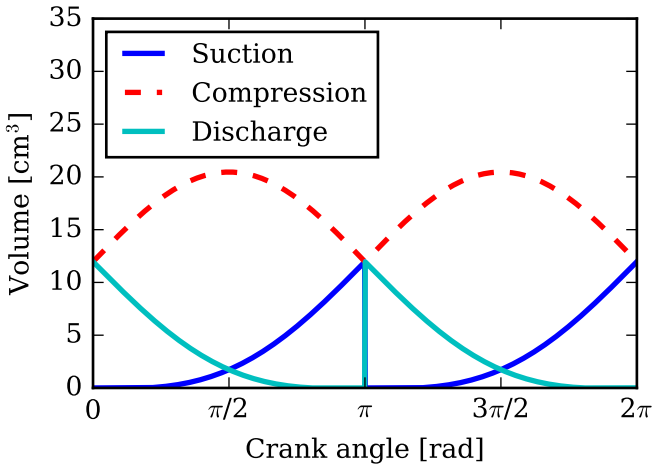

Figure 19: Chamber volume definitions of a spool compressor. To be noted is the discontinuity of suction and compression chambers at π ((Mathison et al., 2013; Bradshaw and Groll, 2013)).

the discontinuity. This numerical technique can be applied to other compressor types that have similar modeling challenges, such as the spool compressor (Bradshaw and Groll, 2013), as shown in Figure 19. The Z-compressor involves continuous interactions between upper chambers and lower chambers via leakage paths. The stiffness of the governing equation is not constant and the adaptive solver decreases the step size to maintain the error within a certain threshold. At π, an even smaller step is enforced to step through the discontinuities of the control volumes and continue the integration.

The Z-compressor presents several leakage paths. For the current design, the main leakage paths are identified in Figure 20. By analyzing the leakage paths, it can be found that most of them present lengths that are relatively long compared to the cross-sectional area. In addition, the leakage path flow area is not always constant. Assuming isentropic flow of perfect gas will overestimate the leakage flows. A detailed 1D-flow model as described by Bell et al. (2013a) is used to determine a correction factor between the mass flow rate of leakage using the detailed flow with friction model and the mass flow rate predicted using a simpler isentropic flow model. For a given configuration, the ratio of the isentropic nozzle mass flow rate prediction to that of the detailed model is defined by

$$M = \frac{\dot{m}_{\text{nozzle}}}{\dot{m}_{\text{fr}}} = \frac{a_0 \left(L/L_0\right)^{a_1}}{a_2 \left(\delta/\delta_0\right) + a_3} \Big\{ \xi \left(a_4 \text{Re}^{a_5} + a_6\right) + \left(1 - \xi\right) \left(a_7 \text{Re}^{a_8} + a_{10}\right) \Big\} + a_{11} \tag{15}$$

where the dimensionless characteristic length and dimensionless gap width are given by $L^* = L/L_0$ and $\delta^* = \delta/\delta_0$ with L_0 and δ_0 being the reference length and gap width values. The correction factors are then used to compute the mass flow rate in and out each control volume during

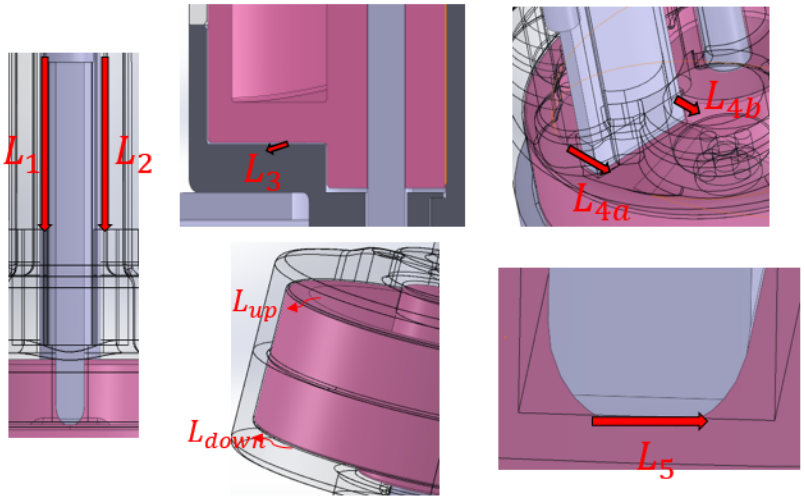

Figure 20: Leakage paths of the Z-compressor.

the integration of the differential equations (Ziviani and Groll, 2017).

The average total shaft power is given by the sum of the compression power, $\overline{\dot{W}}_{\mathrm{pV}}$, and the total friction power losses, $\overline{\dot{W}}_{\mathrm{fr,tot}}$, due to contacts among the different parts,

$$\overline{\dot{W}}_{\mathrm{sh}} = \overline{\dot{W}}_{\mathrm{pV}} + \overline{\dot{W}}_{\mathrm{fr,tot}} \tag{16}$$

A detailed force and moments analysis has been included to estimate the friction losses. In particular, once the pressure distribution within the working chambers is known, radial and axial loads on blade, shaft and bearings can be obtained as well as the associated frictional torques. Each frictional torque multiplied by the rotational speed gives the friction loss power. A comprehensive description of this approach can be found in (Jovane, 2007). The average total friction loss power is given as:

$$\begin{aligned}\overline{\dot{W}}_{\mathrm{fr,tot}} = \sum_i \dot{W}_{\mathrm{i,fr}} = \overline{\dot{W}}_{\mathrm{fr,pt}} + \overline{\dot{W}}_{\mathrm{fr,v}} + \overline{\dot{W}}_{\mathrm{fr,flat}} \\ + \overline{\dot{W}}_{\mathrm{fr,cyl-cyl}} + \overline{\dot{W}}_{\mathrm{fr,cyl-flat}} \\ + \overline{\dot{W}}_{\mathrm{fr,TB}} + \overline{\dot{W}}_{\mathrm{fr,JB-low}} + \overline{\dot{W}}_{\mathrm{fr,JB-up}}\end{aligned} \tag{17}$$

where $\overline{\dot{W}}_{\mathrm{fr,pt}}$ is the friction power associated with the tangential component of the pressure forces acting on the Z-blade, $\overline{\dot{W}}_{\mathrm{fr,v}}$ is the total friction power due to the contact between vane and blade on both sides of the blade, $\overline{\dot{W}}_{\mathrm{fr,flat}}$ is the frictional loss due to the flat portions of the Z-blade, $\overline{\dot{W}}_{\mathrm{fr,cyl-cyl}}$ is the friction loss between the outer cylinder wall and the compressor inner shell, $\overline{\dot{W}}_{\mathrm{fr,cyl-flat}}$ is the friction losses induced by the upper and lower flat circular crowns of the outer cylinder and $\overline{\dot{W}}_{\mathrm{fr,TB}}$, $\overline{\dot{W}}_{\mathrm{fr,JB-low}}$, $\overline{\dot{W}}_{\mathrm{fr,JB-up}}$ are the losses related to thrust bearing, lower and upper journal bearings, respectively.

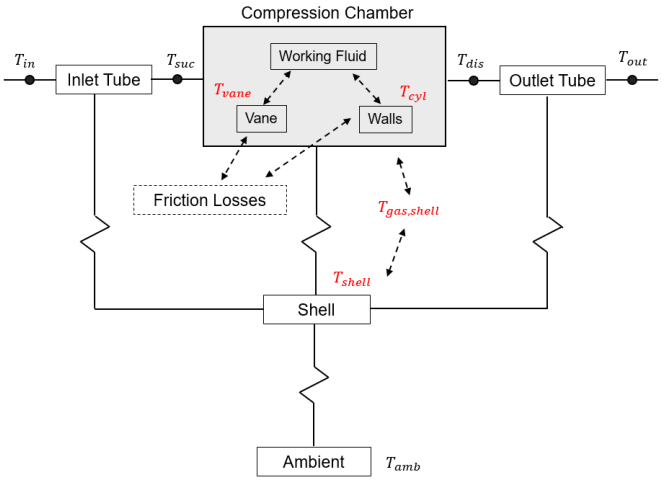

Figure 21: Multi-lump overall energy balance of an open-drive Z-compressor.

The compressor model is closed by enforcing a steady-state overall energy balance with the shell of the compressor. By referring to Figure 21, four lumped element have been identified and the resulting thermal resistance network is shown in Figure 22. By applying the energy conservation law to the compressor components, the following system of energy balance equations can be obtained:

$$\overline{\dot{Q}}_{\mathrm{mass,gas}} - \overline{\dot{Q}}_{\mathrm{CV,wall}} - \overline{\dot{W}}_{\mathrm{fr,flat}} - \overline{\dot{W}}_{\mathrm{fr,tip-seal}} - \overline{\dot{W}}_{\mathrm{fr,pt-blade}} = 0 \tag{18}$$

$$\overline{\dot{Q}}_{\mathrm{shell,amb}} - \overline{\dot{Q}}_{\mathrm{gas-shell,shell}} - \overline{\dot{Q}}_{\mathrm{vane,shell}} - \overline{\dot{W}}_{\mathrm{fr,JB}} - \overline{\dot{W}}_{\mathrm{fr,TB}} = 0 \tag{19}$$

$$\overline{\dot{Q}}_{\mathrm{vane,shell}} - \overline{\dot{Q}}_{\mathrm{CV,vane}} - \overline{\dot{W}}_{\mathrm{fr,vane-cyl}} = 0 \tag{20}$$

$$\overline{\dot{Q}}_{\mathrm{gas-shell,shell}} - \overline{\dot{Q}}_{\mathrm{vane,shell}} = 0 \tag{21}$$

The detailed compressor model developed is used as a tool to investigate the internal behavior of the compressor and to quantify the sources of losses. Figure 23 shows

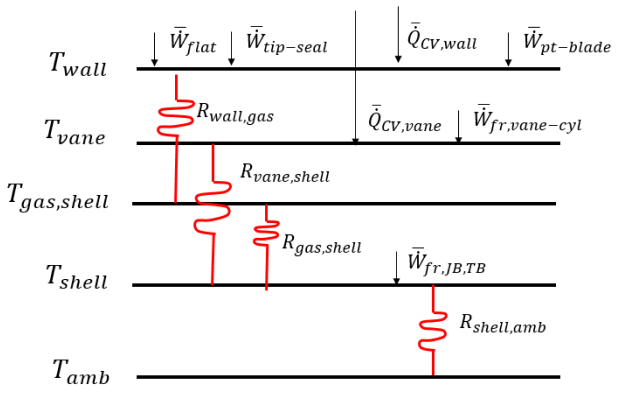

Figure 22: Thermal resistance network of an open-drive Z-compressor .

an example of pressure traces with respect to the rotation angle. The plot of the internal pressure of the compressor during the working process helped adapting the valve parameters to achieve the required operating points.

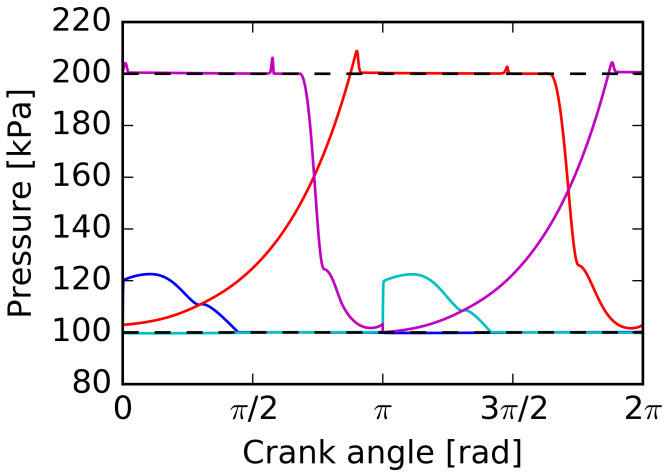

Figure 23: Evolution of the pressure within the working chambers of a Z-compressor throughout one rotation. The colors of the solid lines are identical to the ones in Figure 18.

The Z-compressor model allows to breakdown the frictional losses and the leakage flows to identify potential design improvements. Figure 24 and 25 illustrate the different sources of losses for the baseline design and their magnitude. As described in Ziviani and Groll (2017), the model was exercised to optimize the design and reduce critical losses. In particular, the friction losses between the vane and the blade and the removal of the two journal bearings decreased the mechanical losses of the mechanism. An updated vane design and reduced manufacturing clearances limited the leakage flows through L_4, L_{up} and L_{down}.

4.5. Expander Models

Positive displacement expanders are widely used in ORC applications with power output in the range from 1 kW to

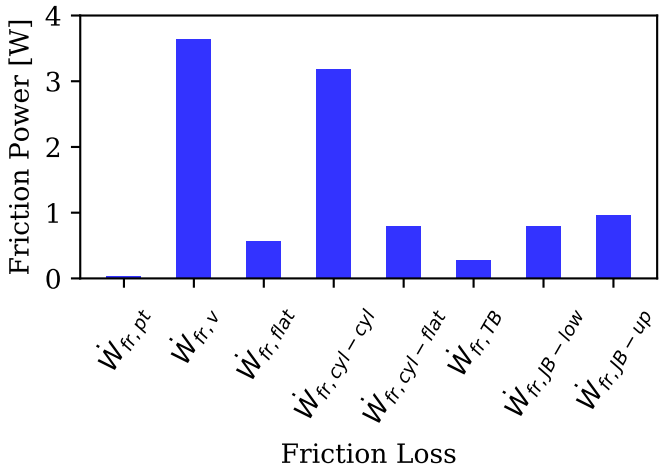

Figure 24: Example of friction loss contributions in an open-drive Z-compressor.

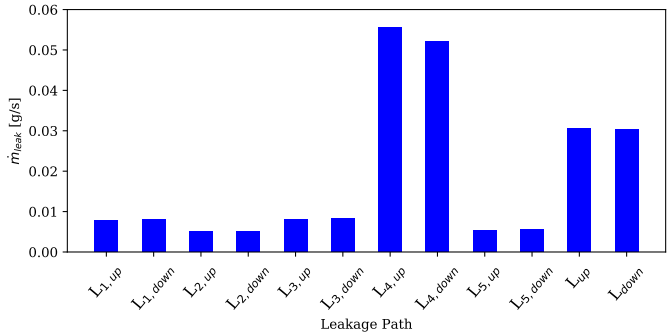

Figure 25: Leakage mass flow rate distribution among all the paths in an open-drive Z-compressor.

500 kW (Macchi and Astolfi, 2016). Since commercially available expanders are limited, compressors are usually modified to operate as expanders, as described in Imran et al. (2016). In PDSim, the mechanistic models developed for reciprocating, rolling-piston and scroll compressors can be easily adapted to operate as expanders by modifying the definitions of the control volumes according to the rotation. The PDSim library already includes examples of reciprocating and scroll expanders.

Among expanders, screw machines are particularly suitable to be employed in the medium to large power output range because of their high isentropic efficiency and favorable trade-off between leakage and friction losses. In the rotary screw family, three main designs can be identified depending on the meshing pair configuration: roots-blower (male-male rotors), twin-screw (male-female meshing pair) and single-screw (central rotor and two gaterotors). The scientific literature about roots expanders is very scarce (Macchi and Astolfi, 2016) due to the fact that the absence of an internal volume ratio makes such machines not suitable for power generation. However, several modeling efforts exist with respect to roots compressors (Mimmi and Pennacchi, 1999, 2001). Instead, twin-screw expanders

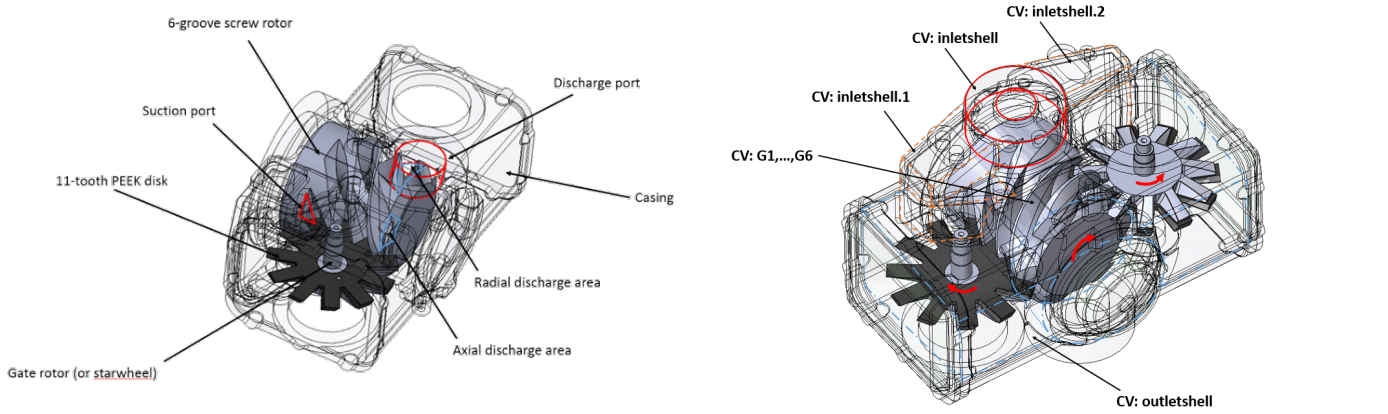

(a) (b)

Figure 26: (a) Description of a single-screw expander and (b) definition of the control volumes.

and compressors are well documented in the open literature (Tang, 1995; Stosic et al., 2005; Papes et al., 2016; Bianchi et al., 2018) and design tools have also been developed, such as SCORPATH (Mujic et al., 2010) and KaSim (Janicki, 2007). The majority of the literature available on single-screw machines deals with compressors (van Male, 1978; Chan et al., 1981; Bein and Hamilton, 1982). More recently, single-screw expanders gained attention as expanders due to their balanced loads on the main rotor. Comprehensive experimental characterizations of single-screw expanders have been published by Ziviani et al. (2016) and Li et al. (2017).

In this work, a single-screw expander is considered as an example of a screw machine implemented in PDSim. However, some of features of the volume curve calculation by means of polygon or the presence of lubricant oil can be applied also to twin-screw machines.

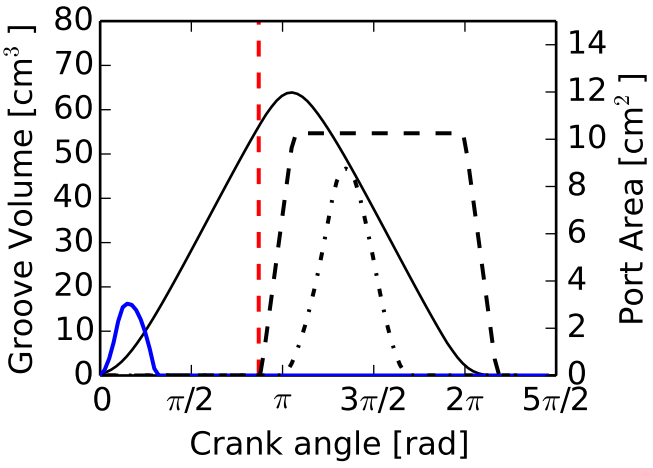

Figure 27: Variation of the groove volume with the crank angle. Suction and discharge ports (radial and axial) are overlaid.

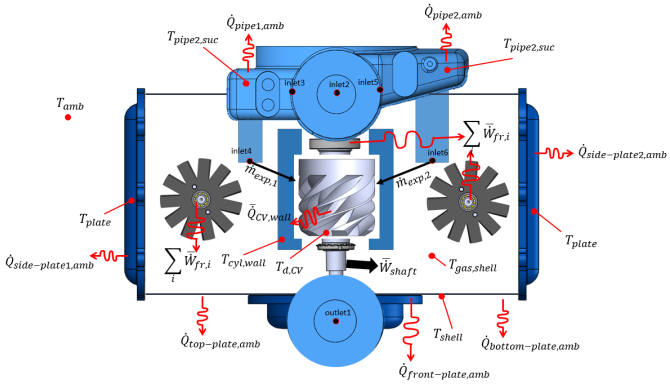

(a)

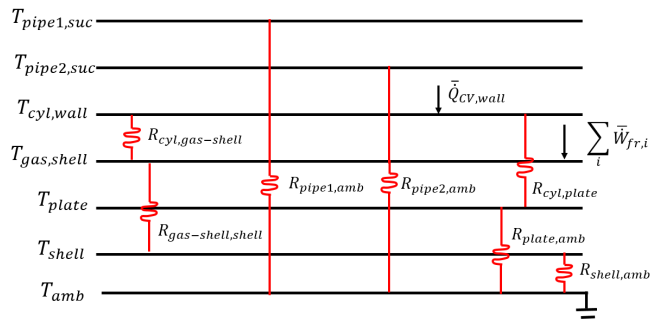

(b)

Figure 28: Schematic of the overall energy balance of the single-screw expander; (b) thermal resistance network of the overall energy balance for single-screw expander (obtained from Ziviani et al. (2018a)).

4.5.1. Single-screw expander

An open-drive single-screw expander for ORC applications is considered. The expander consists of a helically-grooved central rotor with a cylindrical periphery and a globoid core and two identical 11-teeth starwheels engaging with the rotor, as shown in Figure 26(a). Throughout the market history until nowadays, the design config-

uration has always been a 6-groove main rotor and 11-teeth starwheel, although exploratory studies have been conducted on different rotor and gate-rotor configurations as well as number of groove-teeth, as outlined by Ziviani et al. (2018b). The starwheel shafts are parallel to each other with their rotation axes perpendicular to the rotation axis of the main screw. The working chambers are created by the meshing of the starwheels with the main screw rotor grooves. Therefore, the working process occurs simultaneously on both sides of the main rotor, hence the balanced loading. For this reason, the majority of the mechanistic models described in literature consider only one side of the rotor and the geometry model is not defined for a complete working cycle (Bein and Hamilton, 1982; Wang et al., 2016). A more general approach has been adopted by Ziviani et al. (2017). In particular, a non-symmetric description of the machine is considered by computing the expansion process on both sides of the rotor and accounting for potential pressure drops inside the inlet duct. Furthermore, the complete description of the volume curves over one rotation of the main rotor allows to investigate the under- and over-expansion losses. By referring to Figure 26(b), the housing has been divided into four static control volumes (CV) which are associated with the common inlet volume, the two internal ducts that connect the inlet to the suction pockets and shell volume connected to the outlet of the expander. On each side of the rotor, six dynamic control volumes which are changing according to the rotation angle are representative of the six working chambers. The rotation of the main rotor is taken as reference. A polygon-based geometry model has been developed to calculate volume curves, leakage sealing lines, groove surface areas, as described by Ziviani et al. (2018b). The complete groove volume curve and the port areas as a function of the crank angle are shown in Figure 27. A single-screw expander requires lubrication to decrease leakage flows and friction losses. In this case, the oil is mixed with the working fluid. Therefore, the mixture of refrigerant and lubricant oil entering the expander is considered to be homogeneous and at the same pressure and temperature conditions. For a homogeneous mixture, the general mixture thermodynamic property, Ψ_{mix}, is calculated by introducing a liquid mass fraction, x_{oil}:

$$\Psi_{\mathrm{mix}} = x_{\mathrm{oil}}\Psi_{\mathrm{oil}} + (1 - x_{\mathrm{oil}})\,\Psi_{\mathrm{ref}} \tag{22}$$

where Ψ_{oil} and Ψ_{ref} are the properties of lubricant oil and refrigerant, respectively, and with:

$$x_{\mathrm{oil}} = \frac{\dot{m}_{\mathrm{oil}}}{\dot{m}_{\mathrm{oil}} + \dot{m}_{\mathrm{ref}}} \tag{23}$$

Such formulation is applied to obtain mixture specific internal energy, mixture specific enthalpy, mixture specific heat and mixture specific entropy. The thermophysical properties of the refrigerants are retrieved from the CoolProp library (Bell et al., 2014b) by making use of the low-level interface through the *State* class. In the open-literature, lubricant oil property libraries are absent, although lubricant oils are used in most positive displacement compressors and expanders. To close the gap, a *StateFlooded* class derived from the *State* class has been developed and made available open-source within PDSim. This new class works as a container for all the thermophysical properties of refrigerants, lubricant oils and related homogeneous mixtures. The properties of the lubricant oils have been collected from different published sources (Hugenroth, 2006; Zheleznya et al., 2007; Zhelezny et al., 2009b,a; Bell, 2011). The system of governing equations that expresses the conservation of total mass in the control volume, the conservation of the oil mass and the conservation of energy for the general control volume are given as follows:

$$\begin{aligned}
\frac{\mathrm{d}m_{CV}}{\mathrm{d}\theta} &= \frac{1}{\omega}\sum_i \dot{m}_i \\
\frac{\mathrm{d}x_{oil}}{\mathrm{d}\theta} &= \frac{1}{m_{CV}}\left[\frac{1}{\omega}\sum_i \dot{m}_i x_{oil,i} - x_{oil}\frac{\mathrm{d}m_{CV}}{\mathrm{d}\theta}\right] \\
\frac{\mathrm{d}T}{d\theta} &= \frac{1}{m_{CV}c_{v,mix}}\Bigg\{-T\left(\frac{\partial p}{\partial T}\right)_{v_{\mathrm{mix}}}\left[\frac{\mathrm{d}V}{\mathrm{d}\theta} - v\frac{\mathrm{d}m_{CV}}{\mathrm{d}\theta}\right] \\
&-m_{CV}(u_{\mathrm{oil}} - u_{\mathrm{ref}})\frac{\mathrm{d}x_{oil}}{\mathrm{d}\theta} - h\frac{\mathrm{d}m_{CV}}{\mathrm{d}\theta} + \frac{\dot{Q}}{\omega} + \frac{1}{\omega}\sum_i (\dot{m}h)_i\Bigg\}
\end{aligned} \tag{24}$$

To be noted is that the term $\left(\frac{\partial p}{\partial T}\right)_{v_{\mathrm{mix}}}$ must be calculated as a numerical derivative and it cannot be obtained directly from the equation of state unless the oil mass fraction is zero. In the system of equations (24), sub-models for estimating the flow interactions between the working chambers and heat transfer model are necessary in order to carry out the integration, which are described in detail in Ziviani (2017).

The overall energy balance model developed for the single-screw expander is based on previous models applied to rolling piston, scroll and reciprocating compressors (Liu, 1994; Chen, 2000; Kim, 2005). The schematic of the overall energy balance of the single-screw expander and the corresponding thermal resistance network are given in Figure 28(a) and Figure 28(b). As shown in Figure 28(b), there are six unknown temperatures: the shell temperature, $\mathrm{T_{shell}}$; temperature of refrigerant gas in the housing, $\mathrm{T_{gas;shell}}$; side plate temperatures, $\mathrm{T_{plate}}$; suction temperatures, $\mathrm{T_{pipe1;suc}}$ and $\mathrm{T_{pipe2;suc}}$; cylinder wall temperature, $\mathrm{T_{cyl;wall}}$. To be noted is that the temperature of the gas within the shell corresponds to the temperature associated with the control volume *outletshell*. The amount of heat lost to the environment due to natural convection is dependent on the temperature of the housing according to Newton's law of cooling. The resulting system of equations and the heat transfer correlation used can be found in Ziviani et al. (2018a).

The ability of the geometry model to include the re-

turn part of the groove volume while it starts wrapping on the opposite side of the rotor is important for simulating the under- and over- expansion as well as to quantify the flow losses during the discharge process. In Figure 29, the model has been exercised to obtain the p-V diagrams in both cases of under and over-expansion. In particular, the inlet pressure and temperature are fixed at 800 kPa and 100 °C, the rotational speed of the main rotor is 3000 rpm and lubricant oil mass fraction is 0.01. Two values of the discharge pressure have been considered: 150 kPa (case with under-expansion) and 200 kPa (case with over-expansion). These values are also representative of the experimental operating conditions (Ziviani et al., 2016). By comparing the two p-V diagrams, it can be noted that the over-expansion, shown in Figure 29(a), is particularly detrimental for the performance of the machine with respect to under-expansion, shown in Figure 29(b). Under the specified conditions, the slight over-expansion caused a 17% decrease in power output.

5. Conclusions

This work demonstrated the capabilities and the versatility of the first general framework for the analysis of positive displacement compressors and expanders available in the literature, *i.e.*, PDSim, which has been previously described in Bell et al. (2019). The object-oriented coding structure of the software allows easy extension of the existing libraries to model any kind of positive displacement machines. Both steady-periodic and dynamic core equations have been included to enable the simulation of crank-based compressors as well as linear compressors. However, the present work has been limited to crank-based positive displacement machines. Three conventional compressor types, namely reciprocating, scroll, and rotary rolling piston, and a novel Z-compressor have been used to highlight key modeling aspects and numerical challenges. In addition, a single-screw expander has been employed to showcase the capability of implementing expander models. As a result of this work, many researchers, students, and engineers will have access to a powerful tool to further develop compressor and expander technologies.

Acknowledgment

The authors would like to thank the Center of High Performance Buildings (CHPB) at the Ray W. Herrick Laboratories for the financial support.

References

References

Behnel, S., Bradshaw, R., Citro, C., Dalcin, L., Seljebotn, D., Smith, K., 2011. Cython: The best of both worlds. Computing in Science Engineering 13, 31 –39. doi:10.1109/MCSE.2010.118.

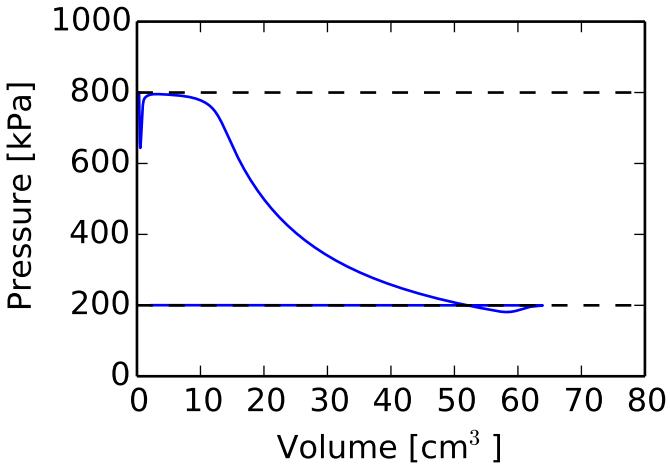

(a)

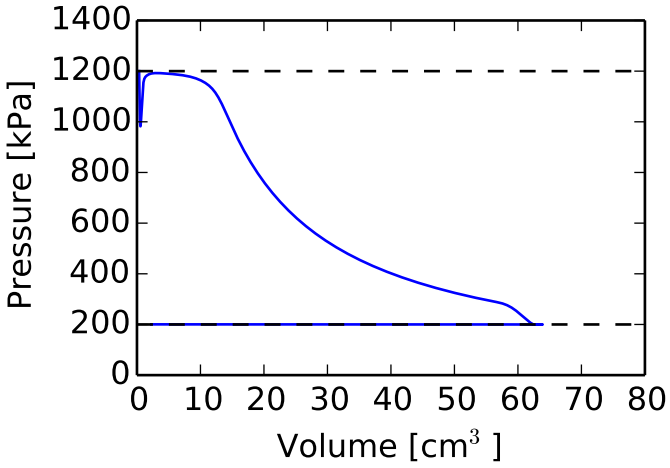

(b)

Figure 29: (a) Pressure versus groove volume of single-screw expander (p_{su}= 800 kPa, T_{su}= 100 °C, x_{oil} = 0.01, N = 3000 rpm): (a) under-expansion (p_{ex}= 150 kPa); (b) over-expansion (p_{ex}= 200 kPa).

Bein, T.W., Hamilton, J.F., 1982. Computer modeling of an oil flooded single screw air compressor, in: 1982 International Compressor Engineering Conference at Purdue University, pp. 127–134.

Bell, I., 2011. Theoretical and Experimental Analysis of Liquid Flooded Compression in Scroll Compressors. Ph.D. thesis. Purdue University. URL: `http://docs.lib.purdue.edu/herrick/2/`.

Bell, I.H., Groll, E.A., Braun, J.E., Horton, W.T., 2013a. A computationally efficient hybrid leakage model for positive displacement compressors and expanders. Int. J. Refrig. doi:10.1016/j.ijrefrig.2013.01.005.

Bell, I.H., Groll, E.A., Braun J., E., Horton, W.T., 2013b. Simulation of a cold climate heat pump furnished with a scroll compressosr with multiple vapor injection llines, in: Proceedings of 8th International Conference on Compressors and their Systems, City University of London, pp. 87–101.

Bell, I.H., Groll, E.A., Braun J., E., Horton, W.T., Lemort, V., 2014a. Comprehensive analytic solutions for the geometry of symmetric constant-wall-thickness scroll machines. International Journal of Refrigeration 45, 223–242.

Bell, I.H., Wronski, J., Quoilin, S., Lemort, V., 2014b. Pure and Pseudo-pure Fluid Thermophysical Property

Evaluation and the Open-Source Thermophysical Property Library CoolProp. Industrial & Engineering Chemistry Research 53, 2498–2508. doi:10.1021/ie4033999, arXiv:http://pubs.acs.org/doi/pdf/10.1021/ie4033999.

Bell, I.H., Ziviani, D., Lemort, V., Bradshaw, C.R., Mathison, M.M., Groll, E.A., Braun, J.E., Horton, W.T., 2019. A general quasi-steady modeling approach for positive displacement compressors and expanders: PDSim Submitted.

Bianchi, G., JKennedy, S., Zaher, O., Tassou, S.A., Miller, J., Jouhara, H., 2018. Numerical modeling of a two-phase twin-screw expander for Trilateral Flash Cycle applications 88, 248–259.

Bradshaw, C.R., Groll, E.A., 2013. A comprehensive model of a novel rotating spool compressor. International Journal of Refrigeration 36, 1974–1981.

Chan, C.Y., Haselden, G.G., Hundy, G., 1981. The HallScrew compressor for refrigeration and heat pump duties. Int. J. Refrigeration 4, 275–280.

Chen, Y., 2000. Mathematical Modeling of Scroll Compressors. Ph.D. thesis. Purdue University.

Chen, Y., Halm, N., Groll, E., Braun, J., 2002a. Mathematical Modeling of Scroll Compressor. Part I- Compression Process Modeling. Int. J. Refrig. 25, 731–750.

Chen, Y., Halm, N., Groll, E., Braun, J., 2002b. Mathematical Modeling of Scroll Compressor. Part II- Overall scroll compressor modeling. Int. J. Refrig. 25, 751–764.

Damle, R., Rigola, J., Perez-Segarra, C.D., Castro, J., Oliva, A., 2011. Object-oriented ssimulation of reciprocating compressors: Numerical verification and experimental comparison. Int. J. Refrig. 34, 1989–1998.

Dutra, T., Deschamps, C.J., 2015. A simulation approach for hermetic reciprocating compressors including elelectric motor modeling. Int. J. Refrig. 59, 168–181.

Gasche, J.L., Andreotti, T., Maia, C.R.M., 2012. A model to predict R134a refrigerant leakage through the radial clearance of rolling piston compressors. Int. J. Refrig. 35, 2223–2232.

Halm, N., 1997. Mathematical Modeling of Scroll Compressors. Master's thesis. Purdue University.

Hamilton, J.F., 1974. Extension of Mathematical Modeling of Positive Displacement Type Compressors. Short Course Text in Ray Herrick Laboratories, School of Mechanical Engineering, Purdue University.

Hu, J., Yang, L., Shao, L.L., Zhang, C.L., 2014. Generic network model of reciprocating compressor. Int. J. Refrig. 45, 107–119.

Hugenroth, J., 2006. Liquid Flooded Ericsson Cycle Cooler. Ph.D. thesis. Purdue University.

Imran, M., Usman, M., B.-S., P., Lee, D.H., 2016. Volumetric expander for low grade heat and waste heat recovery applications. Renewable and Sustainable Energy Reviews 57, 1090–1109.

Incropera, F.P., Dewitt, D.P., 2002. Fundamentals of Heat and Mass Transfer (5th Edition). Wiley.

Janicki, M., 2007. Modellierung und Simulation von Rotationsverdrängermaschinen. Ph.D. thesis.

Jovane, M., 2007. Modeling and analysis of a novel rotary compressor. Ph.D. thesis. Purdue University.

Kim, H., Roh, C.g., Kim, J.k., Shin, J.m., Hwang, Y., Lee, J.k., 2009. An experimental and numerical study on dynamic characteristic of linear compressor in refrigeration system. International Journal of Refrigeration 32, 1536–1543.

Kim, J.H., 2005. Analysis of a Bowtie Compressor with Novel Capacity Modulation. Ph.D. thesis. Purdue University.

Lee, S.J., Shim, J., Kim, K.C., 2015. Development of capacity modulation compressor based on a two stage rotary compressor - part I: Modeling and simulation of compressor perfromance. Int. J. Refrig. 54, 22–37.

Lemort, V., 2008. Contribution to the Characterization of Scroll Machines in Compressor and Expander Modes. Ph.D. thesis. University of Liège.

Lemort, V., Bell, I.H., Groll, E.A., Braun J., E., 2008. Analysis of liquid-flooded expansion using a scroll expander, in: 19th Compressor Engineering Conference at Purdue University. Paper 1323.

Li, G., Wu, Y., Zhang, Y., Zhi, R., Wang, J., Ma, C., 2017. Performance Study on a Single-Screw Expander for a Small-Scale Pressure Recovery System. Energies 10, 1–14.

Link, R., Deschamps, C.J., 2011. Numerical modeling of startup and shutdown transients in reciprocating compressors. International Journal of Refrigeration 34, 1398–1414.

Liu, Z., 1994. Simulation of a Variable Speed Compressor with Special Attention to Supercharging Effects. Ph.D. thesis. Purdue University.

Macchi, E., Astolfi, M. (Eds.), 2016. Organic Rankine Cycle (ORC) Power Systems. Woodhead Publishing. Chapter 12 - Positive displacement expanders for Organic Rankine Cycle systems, Lemort, V., Legros, A., pp. 361-396.

van Male, J., 1978. Monoscrew - a newly developed refrigeration compressor. International Journal of Refrigeration 1, 242–248.

Mathison, M.M., Braun, J.E., Groll, E.A., 2008. Modeling of a two-stage rotary compressor. HVAC&R Research 14, 719–748.

Mathison, M.M., Braun, J.E., Groll, E.A., 2013. Modeling of a novel spool compressor with multiple vapor injection ports 36, 1982–1997.

Mimmi, G., Pennacchi, P., 1999. Analytical model of a particular type of positive displacement blower 213, 517–525.

Mimmi, G., Pennacchi, P., 2001. Compression Load Dynamics in a Special Helical Blower: A Modeling Improvement 123, 402–.

Mujic, E., Kovacevic, A., Stosic, N., Smith, I., 2010. Advanced Design Environment for Screw Machines, in: International Compressor Engineering Conference at Purdue. Paper 1971.

Nakai, H., ino, N., Hashimoto, H., 1996. Piston-ring Lubrication Problems for Refrigeration Compressors Considering Combined Effects of Supply Oil Quantity and Surface Roughness. Journal of Tribology 118, 286–291.

Ooi, K., Wong, T., 1997. A computer simulation of a rotary compressor for household refrigerators. Applied Thermal Engineering 17, 65–78.

Ooi, K.T., 1992. A real gas simulation of a refrigeration compressor and its performance comparison for CFCs and Non-CFCs, in: International Compressor Engineering Conference at Purdue, p. Paper 872.

Ooi, K.T., Chai, G.B., Kwek, E.C., 1992. A simple valve model to study the performance of a small compressor, in: International Compressor Engineering Conference at Purdue, p. Paper 803.

Pandeya, P.N., 1978. Performance analysis of positive displacement refrigerating compressors. Ph.D. thesis. Purdue University.

Papes, I., Degroote, J., Vierendels, J., 2016. Development of a thermodynamic loworder model for a twin-screw expander with emphasis on pulsations in the inlet pipe. Applied Thermal Engineering 103, 909–919.

Prankash, R., Singh, R., 1974. Mathelatical Model and Simulation of Refrigeranting Compressors, in: 1974 International Compressor Engineering Conference at Purdue University.

Soedel, W., 1972. Introduction to Computer Simulations of Positive Displacement Type Compressors. Short Course Text in Ray Herrick Laboratories, School of Mechanical Engineering, Purdue University.

Soedel, W., 2007. Sound and Vibrations of Positive Displacement Compressors. CRC Press Taylor & Francis Group.

Stiaccini, I., Galoppi, G., Ferrari, L., 2016. A reciprocating compressor hybrid model with acoustic FEM characterization. Int. J. Refrig. 63, 171–183.

Stosic, N., Smith, I., Kovacevic, A., 2005. Screw Compressors - Mathematical Modelling and Performance Calculation. Springer.

Stosic, N., Smith, I.K., Kovacevic, A., Mujic, E., 2011. Review of Mathematical Models in Performance Calculation of Screw Compressors. International Journal of Fluid Machinery and System 4, 271–288.

Tang, Y., 1995. Computer Aided Design of Twin Screw Compressors. Ph.D. thesis.

Wang, Z., Wang, Z., Wang, J., Jiang, W., Feng, Q., 2016. Theoretical and experimental study on thermodynamic performance of single screw refrigeration compressor with Multicolumn Envelope Meshing Pair. Applied Thermal Engineering 103, 139–149.

Wu, J., Chen, A., 2015. A new structure and theoretical analysis on

leakage and performance of an oil-free R290 rolling piston compressor. International Journal of Refrigeration 49, 110–118.

Yanagisawa, T., Shimizu, T., 1985a. Friction losses in rolling piston type rotary compressors. III. Int. J. Refrig. 8, 159 – 165. doi:10.1016/0140-7007(85)90156-2.

Yanagisawa, T., Shimizu, T., 1985b. Leakage losses with a rolling piston type rotary compressor. i. radial clearance on the rolling piston. Int. J. Refrig. 8, 75 – 84. doi:10.1016/0140-7007(85)90077-5.

Yanagisawa, T., Shimizu, T., 1985c. Leakage losses with a rolling piston type rotary compressor. II. Leakage losses through clearances on rolling piston faces. Int. J. Refrig. 8, 152 – 158. doi:10.1016/0140-7007(85)90155-0.

Yanagisawa, T., Shimizu, T., Chu, I., Ishijima, K., 1982. Motion analysis of rolling piston in rotary compressor, in: International Compressor Engineering Conference at Purdue, p. Paper 392.

Yang, B., Bradshaw, C.R., Groll, E.A., 2013. Modeling of a semi-hermetic CO_2 reciprocating compressor including lubrication submodels for piston rings and bearings. Int. J. Refrig. 36, 1925–1936.

Yang, B., Zhao, Y., 2013. Piston ring-cylinder linline lubrication analysis in a CO_2 refrigeration reciprocating compressor. Inst. of Mech. Eng., Part C: J. Mech. Eng. Sci. 225, 2638–2648.

Yang, B., Ziviani, D., Groll, E., 2017. Comprehensive model of an hermetic reciprocating compressor. IOP Conf. Ser.: Mater. Sci. Eng. 232.

Zhang, H., Wu, J., Xie, F., Chen, A., Li, Y., 2014. Dynamic behaviors of the crankshafts in single-cylinder and twin-cylinder rotary compressors. International Journal of Refrigeration 47, 36–45.

Zhang, X., Ziviani, D., Groll, E.A., Braun, J.E., 2017. A Numerical Study on Dynamic Characteristics of Linear Compressor for Electronics Cooling, in: 8th International Conference on Compressors and Refrigeration (ICCR), Xi'an Jiaotong University. F22.

Zhelezny, V.P., Nichenko, S.V., Semenyuk, Y.V., Kosoy, B.V., Kumar, R., 2009a. Influence of compressor oil admixtures on theoretical efficiency of a compressor system. International Journal of Refrigeration 32, 1526–1535.

Zhelezny, V.P., Sechenyh, V.V., Semenyuk, Y.V., Grebenkov, A.J., Beliayeva, O.V., 2009b. An experimental investigation and modelling of the viscosity refrigerant/oil solutions. International Journal of Refrigeration 32, 1389–1395.

Zheleznya, V., Semenyuka, Y., Ancherbaka, S., Grebenkovb, A., Beliayevab, O., 2007. An experimental investigation and modelling of the solubility, density and surface tension of 1,1,1,3,3-pentafluoropropane (r-245fa)/synthetic polyolester compressor oil solutions. Journal of Fluorine Chemistry 128, 10291038.

Zhou, W., Kim., J., Soedel, W., 2001. New Iterative Scheme in Computer Simulation of Positive Displacement Compressors Considering the Effect of Gas Pulsations . Journal of Mechanical Design 123, 282–288.

Ziviani, D., 2017. Theoretical and Experimental Characterization of Single-Screw Expanders for ORC Applications. Ph.D. thesis.

Ziviani, D., De Paepe, M., Braun, J.E., Groll, E.A., 2018a. Detailed Thermal Model of Open-Drive Single-Screw Expanders for ORC Applications, in: International Compressor Engineering Conference at Purdue University.

Ziviani, D., Groll, E., 2017. Modeling and analysis of an open-drive Z-compressor. IOP Conf. Ser.: Mater. Sci. Eng. 232.

Ziviani, D., Groll, E., Braun, J., De Paepe, M., 2018b. Review and update on the geometry modeling of single-screw machines with emphasis on expanders. International Journal of Refrigeration 92, 10–26.

Ziviani, D., Groll, E., Braun, J., Horton, W., De Peape, M., van den Broek, M., 2017. Non-symmetric approach to single-screw expander and compressor modeling. IOP Conf. Ser.: Mater. Sci. Eng. 232.

Ziviani, D., Sergei, S., Lecompte, S., Groll, E.A., Braun, J.E., Horton, W.T., van den Broek, M., De Paepe, M., 2016. Characterizing the performance of a single-screw expander in a small-scale organic Rankine cycle for waste heat recovery. Applied Energy 181, 155–170.